SCIENTIFIC REPORTS

OPEN

SUBJECT AREAS:
GLYCOBIOLOGY
PRE-CLINICAL STUDIES

Received
11 July 2013

Accepted
8 October 2013

Published
25 October 2013

Correspondence and requests for materials should be addressed to G.N. (navon@post.tau.ac.il)

Molecular imaging of tumors and metastases using chemical exchange saturation transfer (CEST) MRI

Michal Rivlin[1], Judith Horev[2], Ilan Tsarfaty[2] & Gil Navon[1]

[1]School of Chemistry, Tel Aviv University, Tel Aviv, Israel, [2]Department of Clinical Microbiology and Immunology, Sackler School of Medicine, Tel Aviv University, Tel Aviv Israel.

The two glucose analogs 2-deoxy-D-glucose (2-DG) and 2-fluoro-2-deoxy-D-glucose (FDG) are preferentially taken up by cancer cells, undergo phosphorylation and accumulate in the cells. Owing to their exchangeable protons on their hydroxyl residues they exhibit significant chemical exchange saturation transfer (CEST) effect in MRI. Here we report CEST-MRI on mice bearing orthotopic mammary tumors injected with 2-DG or FDG. The tumor exhibited an enhanced CEST effect of up to 30% that persisted for over one hour. Thus 2-DG/FDG CEST MRI can replace PET/CT or PET/MRI for cancer research in laboratory animals, but also has the potential to be used in the clinic for the detection of tumors and metastases, distinguishing between malignant and benign tumors and monitoring tumor response to therapy as well as tumors metabolism noninvasively by using MRI, without the need for radio-labeled isotopes.

Most cancer cells are characterized by high rate of glycolysis even in the presence of oxygen (the "Warburg effect"[1]). This characteristic distinguishes between benign tissue and rapidly growing malignant tumors and is further enhanced in metastatic tumors[2,3]. The two glucose analogues, 2-deoxy-D-glucose (2-DG) and 2-fluoro deoxy-D-glucose (FDG) are taken up by cells through the glucose transporter, and undergo phosphorylation catalyzed by hexokinase. However unlike glucose they and their metabolic products accumulate in the cells[4,5]. This property is the basis of the use of the radioactive ^{18}F-FDG for positron emission tomography (PET)[6–9]. At present, the vast majority (~95%) of all clinical PET studies use FDG. Usually PET is not used as a stand-alone modality but is combined with computerized tomography (PET/CT). Recently combined PET/MRI scanners were developed[10,11], however, their clinical use is still in its infancy. Obviously, if magnetic resonance imaging of the FDG molecules was possible it would have been a valuable alternative to the PET/MRI combination. Nakada et al[12] and Kanazawa et al[13] suggested the MR imaging of FDG using its natural stable isotope ^{19}F. They demonstrated the ^{19}F MRI of FDG in rat brain, but due to the low SNR this approach would not be practical for clinical application.

The chemical exchange saturation transfer (CEST) NMR method enables to detect low concentrations of metabolites that contain residues with exchangeable protons such amine, amide or hydroxyl[14,15]. The enhanced sensitivity of the method allows obtaining images of relatively low concentrations of endogenous cellular components or exogenous agents by MRI. Enhancement factors of up to 10^6 relative to the concentration of the molecules of interest have been reported for certain systems (For recent reviews see e.g.[16–18]). CEST has been shown to enable the imaging of tissue pH[19], to map brain proteins through their –NH residues[20], to monitor glycogen concentration in the liver[21], to image myo-inositol in the brain[22] and to map a specific gene expression *in vivo*[23]. By the use of CEST we were able to image changes of the levels glycosaminoglycans (GAGs) in human joints *in vivo* following injury[24] and also to follow changes on the GAGs contents in the nucleus pulposus part of intervertebral discs *in vitro*[25]. Recently, CEST measurements were reported for implanted tumors in mice following administration of glucose (glucoCEST)[26,27] and for rat brain following administration of 2-DG[28].

In the present work we take advantage of the enhanced accumulation of 2-DG and FDG in tumors to obtain high CEST values. Our results suggest that either 2-DG-CEST or FDG-CEST could serve as potential replacements of PET/CT or PET/MRI in the clinic for the detection of tumors and metastases, distinguishing between malignant and benign tumors and monitoring tumor response to therapy, without the need for radio-labeled isotopes.

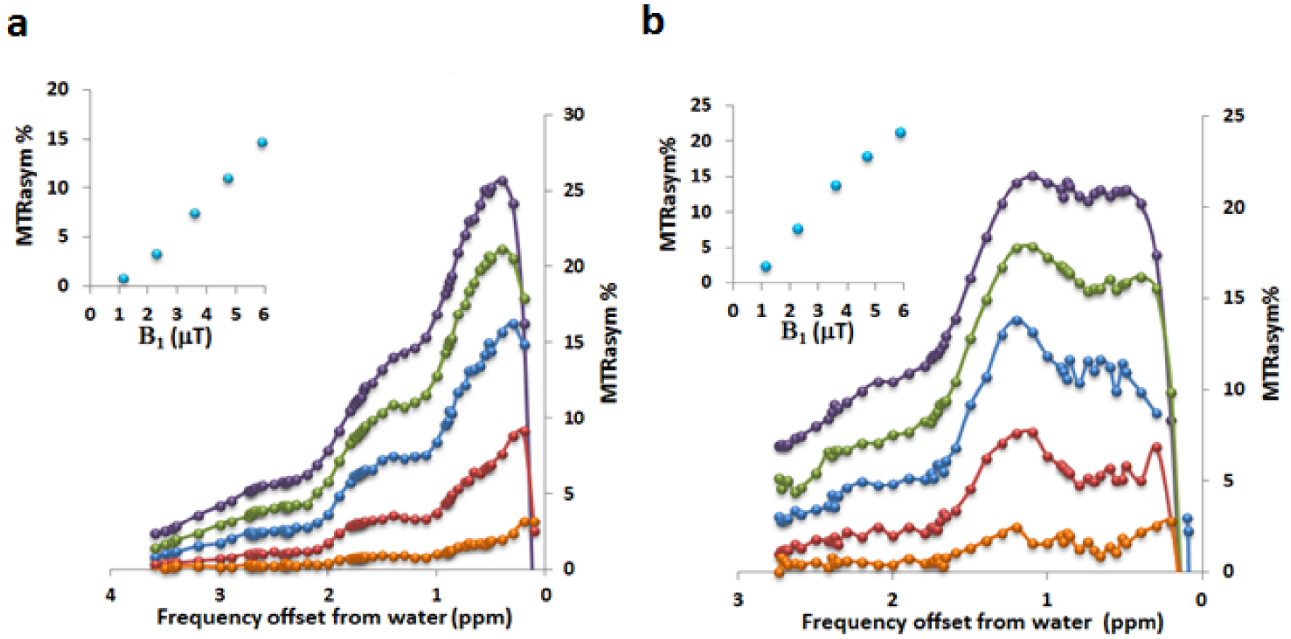

Figure 1 | MTRasym plots of 20 mM FDG (a) and 2-DG-6P sodium salt (b) in H_2O solution (10% D_2O) as a function of rf saturation field (B_1) at pH = 6.3 (a)and 7.5(b), T = 25°C, at 11.7 T. The inserts are the MTR_{asym} plots at 1.2 ppm vs. rf saturation field B_1 (μT).

Results

The magnitude and the frequency dependence of the CEST effect were measured for the two glucose analogs, FDG, 2-DG and for the phosphorylated derivative of 2-DG, as potential markers of tumor response. The MTR_{asym} plots for FDG and 2-DG-6P at a concentration of 20 mM are shown Fig. 1. The CEST percent increased with the B_1 power and, for the peak at 1.2 ppm, reached values of 15% and 22% for FDG and 2-DG-6P respectively for B_1 power level of 5.9 μT (250 Hz). The CEST for 2-DG was about 30% lower than that of 2-DG-6P. It may be noted that no hydroxyl proton peaks could be observed for the same solutions by ^{1}H NMR single pulse experiment. This is explained by the fact that since the water proton concentration is 111 M, CEST values of about 20% for 20 mM concentrations of the glucose analogs correspond to an enhancement factor of about 10^3 over the direct detection of the metabolites. The CEST experiment was also done for 2-DG-6P in D_2O solution in order to obtain a better resolved spectrum (not shown here). In this experiment the MTR_{asym} plot shows well resolved three peaks belonging to hydroxyl protons at about 1.2, 2.1 and 2.8 ppm. A forth peak may be present at about 0.6 ppm from the water resonance. The CEST effect of a combined extracts of tumors following the i.v. injection of 1–4 g/kg 2-DG shown in Fig. 2(b) has similar features as those of 2-DG and 2-DG-6P solutions. Fig. 2(a) show the CEST effect for solution made of pooled extracts of several tumors with no 2-DG injection showing lower values of CEST.

^{19}F NMR studies. In order to assess the fate of FDG after being introduced to the tumor, ^{19}F NMR was measured on combined extracts of tumors excised at 60–90 min. after administration of FDG (Fig. 3). It is seen from the figure that the ratio of the fraction of FDG that underwent phosphorylation to that of the unphosphorylated one is 0.76 : 1. This value was calculated for the ratio of the α anomers whose spectra are well resolved. One can assume that the same ratio applies also for the β anomers since the ratio

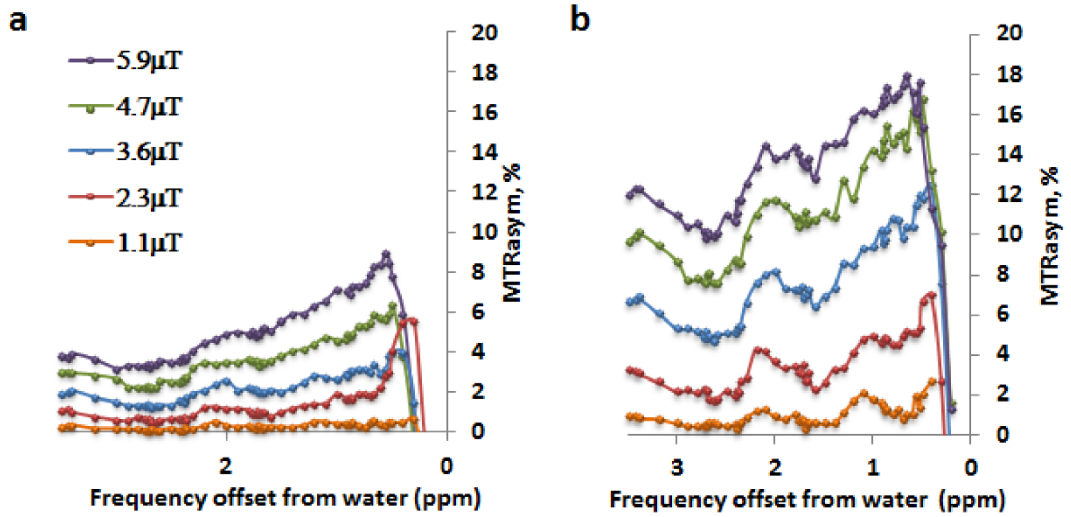

Figure 2 | MTRasym plots of combined extracts of tumors (with 10% D_2O) as a function of rf saturation field (B_1) at pH = 7.5, T = 25°C, at 11.7 T: (a) combined control extracts of tumors; (b) combined extracts of tumors treated with 2-DG.

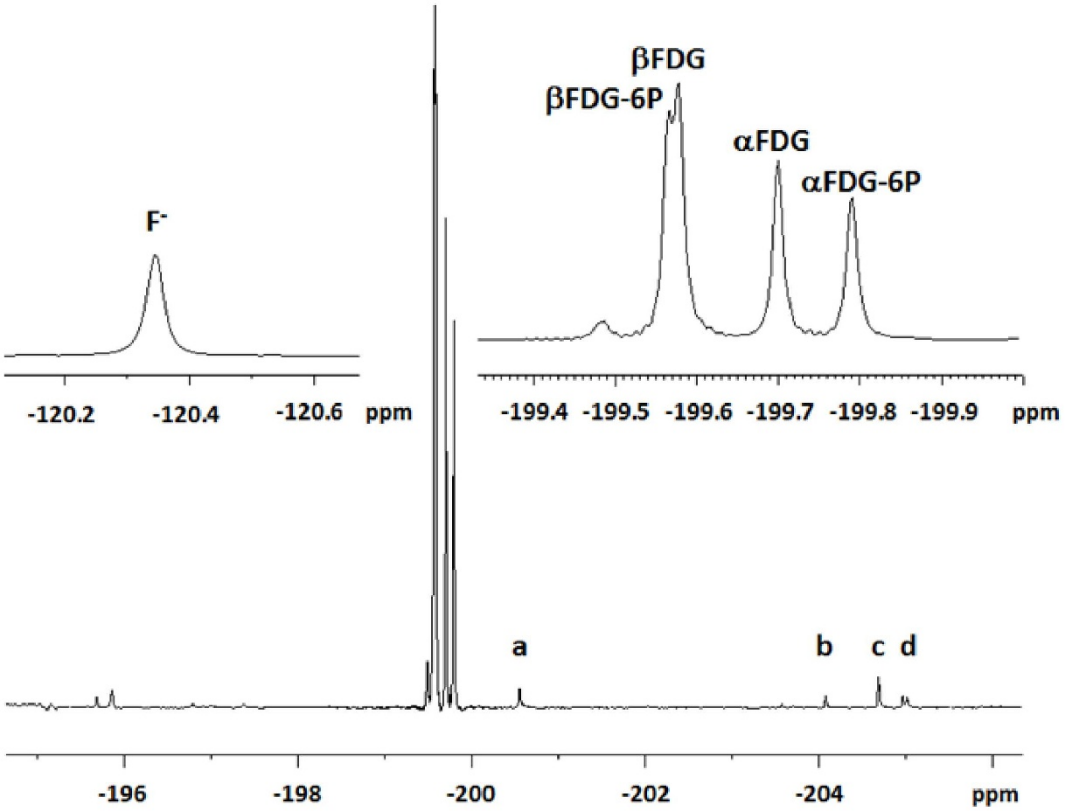

Figure 3 | **^{1}H-decoupled ^{19}F NMR spectrum of combined extracts of tumors injected with FDG.** Signals assignments were based on previously published data[29]. (a): UDP-FDG; (b): αFDM-1P; (c) αFDM-6P; (d) UDP-FDM and αFDM. The peaks are referenced to $CFCl_3$ in $CDCl_3$ (0 ppm).

between the α and β anomers is not sensitive for the phosphorylation at the 6th position (Rivlin et al., unpublished results). Based on the similar CEST effects for 2-DG and 2-DG-6P both FDG and FDG-6P should have equal contributions to the CEST and thus for the tumor the ratio of the phosphorylated to unphosphorylated FDG is about 0.76 : 1. Other metabolic products of FDG such as FDM, FDM-6P may also contribute to the CEST of the tumor, but their concentrations are relatively small. One metabolic product that was not reported before is inorganic fluoride ion. However this product should not contribute to the CEST effect but will contribute to the PET images.

***In vivo* CEST MRI studies.** To study the potential use of CEST MRI to image mammary tumors, we performed 2-DG/FDG CEST MRI experiments on mice bearing DA3 tumors injected with either 2-DG or FDG glucose analogs. Tumor anatomy was initially imaged using T_2 weighted spin echo sequence (RARE). The MR images prior to glucose analog injection showed CEST effects in the tumor at a shift of $\pm$1.2 ppm relative to the water signal and B_1 value of 2.5 μT (106 Hz) in the range of 6.1 $\pm$ 1.4%, n = 6.

Three examples of CEST-MR images of tumors following the administration of the 2-DG or FDG are given in Figs. 4–6. In the first experiment 2-DG was administered by cannulation via the tail vein and in the last two by i.v. injections. As it can be seen from Fig. 4, 12 min after the 2-DG injection (2 g/kg) a strong CEST effect was visualized at the tumor, which can be attributed to a combination of the accumulation in the tumor of 2-DG, and its phosphorylated products. The temporal change in %CEST showed rapid increase up to about 0.5 hours following by long steady state persistence of the CEST effect at a level of 22%. A second dose of 2 g/kg 2-DG resulted in a further increase of the CEST effect. Other organs (apart from the urinary bladder) did not show any significant CEST effect throughout the MRI scans session. It is interesting to note that only the lower part of the tumor displayed CEST effect. Presumably only this part has an active metabolism. Fig. 5 describes an experiment where a large necrotic area was present at the center of the tumor. The CEST effect was most pronounced at the rim of the tumor, presumably the most metabolic active part. In this experiment the CEST had sharp increase at 4 min and a steady increase up to 90 min. The difference in the initial temporal behavior may be related to the method of the 2-DG administration. In Fig. 6, CEST images following the injection of 1 g/kg FDG are described. Here again, like the second 2-DG experiment there was a sharp CEST increase within less than 12 minutes. In this particular experiment the CEST effect in the control was unusually high (12%). However the CEST at about 1 hour following the injection of FDG was much higher (30%).

As was mentioned in the Introduction, CEST measurements were performed in implanted tumors in mice following administration of glucose (glucoCEST)[26,27]. To compare 2-DG/FDG-CEST to glucoCEST under the same experimental setups we performed experiments using injection of 1.5 g/kg glucose. The results of the experiments were essentially the same and one of them is shown in Fig. 7. As can be seen from the figure the two main differences between the glucose experiment and those of the 2-DG and FDG glucose analogs are the lower CEST enhancement by the glucose, which was of about 10% at its maximum, and the sharp decline of the CEST after 20 minutes reaching a value of only 3% above the control. This is in contrast with the CEST of 2-DG and FDG which persisted for over an hour.

Discussion

This study has shown that 2-DG/FDG CEST detection is feasible in tumor of mice at 7 T. The tumor exhibited CEST enhancements of up to 30% for mice injected with either 2-DG or FDG. These high values are the combined results originate from the injected 2-DG and

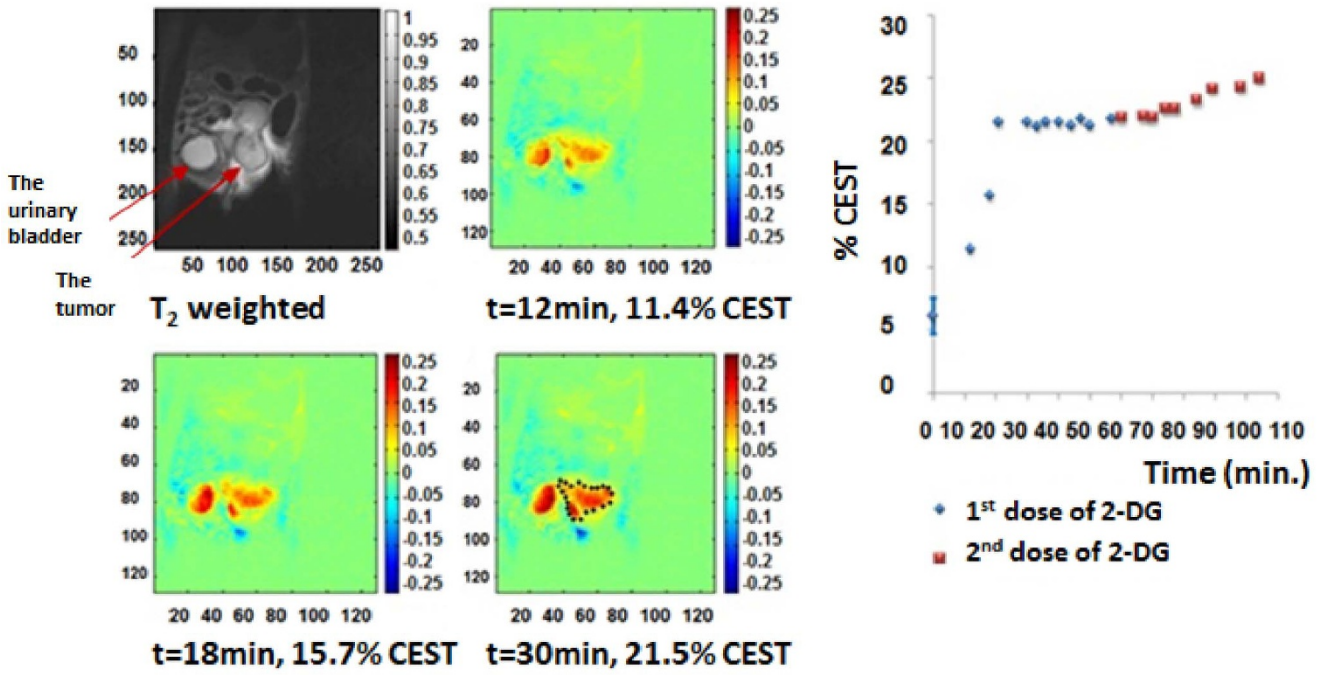

Figure 4 | **CEST MRI kinetic measurements in the tumor at different times following 2-DG treatment.** Each injection was 2 g/kg body weight. In gray scale, the conventional T_2 weighted image (before injection). The marked ROI was used for the %CEST calculation.

FDG, their phosphorylated products 2-DG-6P and FDG-6P and from other metabolic products. This conclusion is based on our ^{19}F NMR of the extracts of the excised tumors following the administration of FDG showing that more than half of the FDG in the tumors remained in the unphosphorylated form. Reports in the literature indicate that FDG-5P is partially converted to 2-fluoro-2-deoxy-D-mannose 6-phosphate (FDM-P) in rodents brain, heart and tumors[13,29–32]. The rate of phosphorylation of 2-DG is similar to that of FDG measured in the present work. This conclusion is based on our previous in vivo ^{13}C NMR results obtained for implanted MCF-7 tumors in mice following i.p. injection of 2-DG labeled at the 6th position[33]. In that study the concentration of 2-DG-6P reached the same level as that of the 2-DG at about 90 min and after 250 min most of the 2-DG has disappeared while the 2-DG-6P retained about half of its maximal value. 2-DG was found to convert in rat brain, in addition to 2-DG-6P also to 2-deoxy-D-glucose1-phosphate and 2-deoxy-D-glucose1,6-biphosphate[34]. The CEST effect of the phosphorylated and the unphosphorylated sugars do not differ that much.

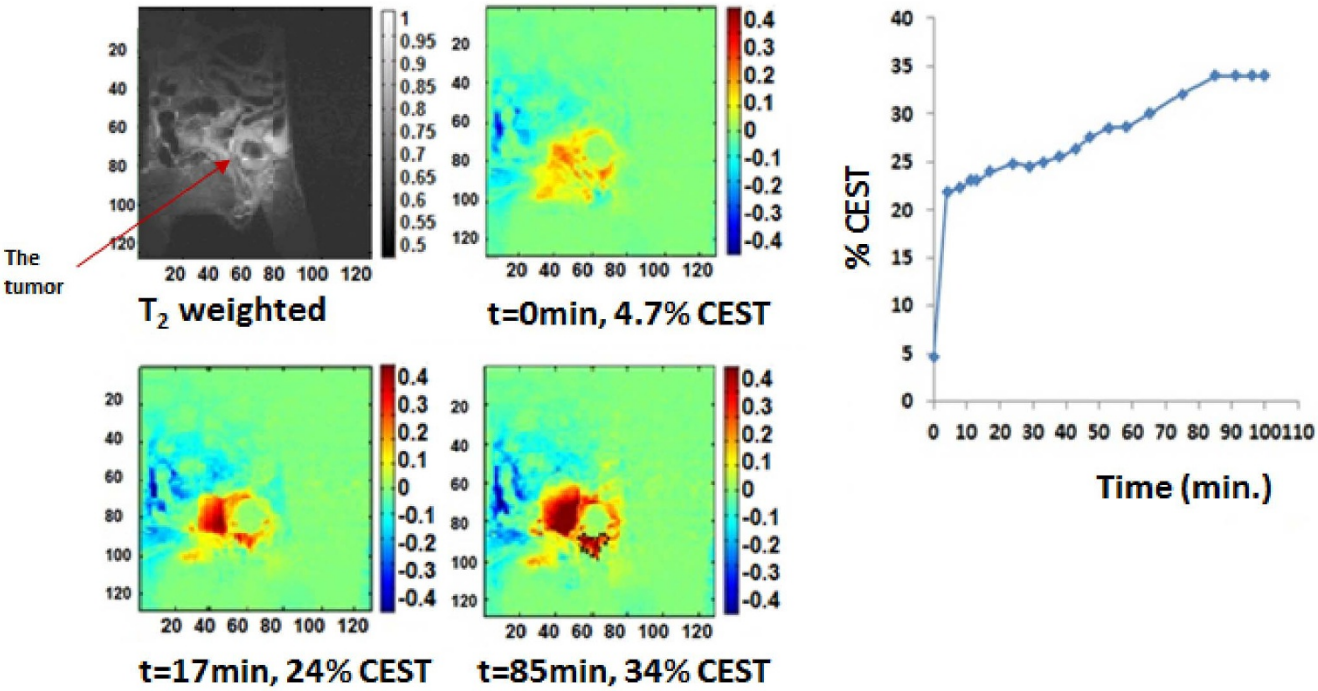

Figure 5 | **CEST MRI kinetic measurements in the tumor at different times following injection of 2-DG, 1 g/kg.** The upper left image is T_2 weighted image that identifies the location of the tumor prior to administration of 2-DG. The marked ROI was used for the %CEST calculation.

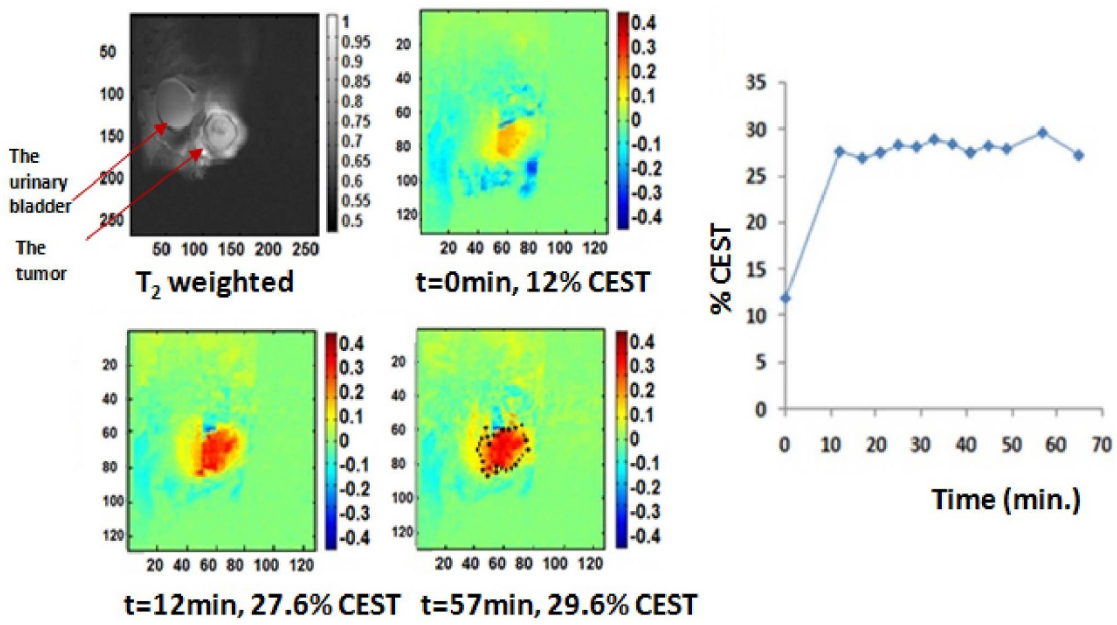

Figure 6 | CEST MRI kinetic measurements in the tumor at different times following injection of FDG, 1 g/kg. The upper left image is T_2 weighted image that identifies the location of the tumor prior to administration of FDG. The marked ROI was used for the %CEST calculation.

The CEST effect of 2-DG-6P was found by us and in ref. 28 to be about 30% greater than that of 2-DG. The lower CEST effect following injection of glucose and its short duration is not surprising since glucose is expected to be further metabolized to lactic acid that arbor no CEST effect.

Tumor tissue is not homogeneous, containing clusters of tumor and normal cells, vascular structures and necrotic tissue. Our FDG/2-DG CEST MRI demonstrates this heterogeneity. Only the metabolically active part of the tumor exhibit enhanced CEST effect, this illustrates the diagnostic benefit and uniqueness of this technique that is sensitive enough to detect regional differences in tumor uptake. Unlike the conventional anatomical images, 2-DG CEST MRI method enables to distinguish between the demand parts of tumor, while no CEST signal is obtained from the necrotic region or other non-metabolically active parts of the tumor.

This method has the potential to detect even small tumors in patients, by 2-DG or FDG uptake, based on differences in the contrast. Clear advantage to this method can be expressed in monitoring patient after chemotherapy, and compare the CEST contrast obtained by normal and tumor tissue.

The use of 2-DG and FDG CEST in studies of cancer in laboratory animals seems to be straightforward and has a great promise to become a standard tool for experimental cancer research. As for human clinical use, glucoCEST could have the advantage of administration of glucose instead of 2-DG or FDG. However the low values[26,27] and the short duration of glucoCEST enhancements must be a serious obstacle for its potential future clinical application. The use of 2-DG in human clinical diagnosis seems possible in view of the past and ongoing clinical trials for its therapeutic usage, either as a single agent or in combination with other therapeutic modalities[35].

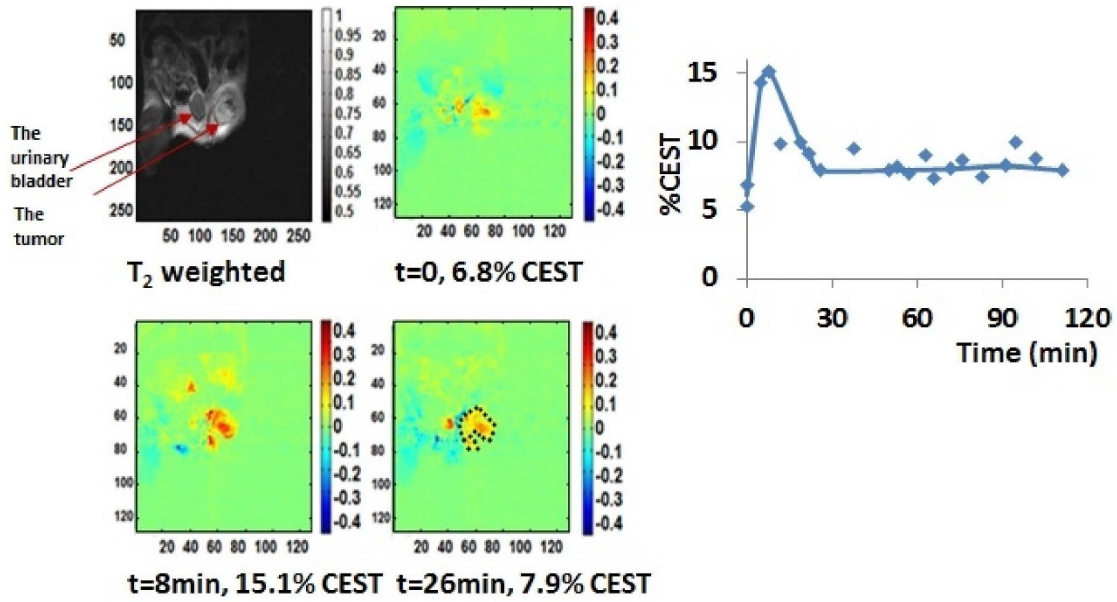

Figure 7 | CEST MRI kinetic measurements in the tumor at different times following injection of D-glucose, 1.5 g/kg. The upper left image is T_2 weighted image that identifies the location of the tumor prior to administration of D-glucose. The marked ROI was used for the %CEST calculation.

For example, there are reports of a phase I/II trial with 2-DG alone in patients with castrate-resistant prostate cancer[36], or phase I trial of 2-DG alone or combined with docetaxel in patients with advanced solid tumors[37]. In clinical trials that used 2-DG to improve the efficacy of radiotherapy, 200–300 mg 2-DG per kg body weight were orally administered after overnight fasting, with either minor or no side effects[38].

We expect that the developed novel imaging modality will enable early detection of tumors, tumor response to therapy, and tumors metabolism noninvasively by using MRI, without the need for radiolabeled isotopes. This novel imaging modality will also shed a new light on tumor basal metabolism, expression of tumor markers and the metabolic alteration induced by constitutive activation of oncogenes in tumor development.

Methods

1. **Chemicals and Media:** 2-DG and 2-DG-6P sodium salt were obtained from Sigma-Aldrich, Israel; FDG was obtained from Carbosynth Limited, UK.
2. **Cells:** DA3-D1-DMBA-3 is a cell line derived from a poorly differentiated mammary adenocarcinoma induced in BALB/C mice by dimethylbenzanthracene[39].
3. **Animals:** BALB/C female mice were purchased and kept in the breeding facility of the Sackler School of Medicine, Tel Aviv University. To induce orthotropic tumors in mice, DA3 cells were injected into the lower left mammary gland of 8 week old (17–22 gr) female BALB/c mice (5×10^5 cells in 100 μL saline).
   All experiments with animal models were done in compliance with the principles of the National Research Council (NRC) and were approved by the institutional animal care and use committee (IACUC) (#M-12-035).
4. **Preparation of Tumor Extracts:** The tumors were surgically excised and weighed quickly and immediately immersed in liquid nitrogen. The frozen tumors were homogenized using a tissue homogenizer with 0.4 ml of 5.5 M precooled (-10°) perchloric acid to every 0.1 gr of tumor. Samples were centrifuged at 3500 × g and -4°C for 20 min and the pH of the supernatant was adjusted to pH = 6.5–7 with RbOH (50%) in an ice water bath. The precipitated rubidium perchlorate was removed by a second centrifugation at 6000 × g and -4°C for 12 min. The choice of RbOH instead of the commonly used KOH was because of the lower solubility of $RbClO_4$ relative to the potassium analog and its larger density which assist in its separation by centrifugation. The supernatant was passed through Chelex chelating ion exchange resin (pH = 7.0) in order to eliminate paramagnetic impurities and the pH was adjusted to 6.5–7. The samples were frozen at -20°C, and lyophilized to dryness for 24 hr. Each supernatant was dissolved in 0.5 ml D_2O (99.98%, Biolab, Israel) and inserted into 5 mm tube for ^{19}F and ^{1}H NMR.
5. **NMR Spectroscopy:** ^{1}H NMR Spectra were recorded at 500 MHz in 5 mm tubes on a Bruker 500 MHz DRX with the following parameters: spectral width 7500 Hz, pulse width 5.5 us (corresponding to a 45° flip angle); data size 16 K; relaxation delay 7 s; number of scans = 16. ^{19}F NMR spectra were recorded at 470.5 MHz in 5 mm tubes using a 500 MHz AVANCE3. Acquisition parameters were as follows (for the perchloric acid extracts): spectral width 9.5 KHz, data size 32 K, pulse width 3.2 us (30° flip angle); relaxation delay 1 s; number of scans = 60,000.
6. **CEST NMR** experiments were performed by applying a long off-resonance presaturation pulse before acquisition. A series of frequencies (Ω) were used in the range of −3.5 to +3.5 ppm relative to the water signal. Several B_1 powers in the range of 1–6 μT (~50–250 Hz) and durations of 2 s were used. The chemical exchange contrast was measured by magnetization transfer asymmetry, MTRasym:

$$MTR_{asym}(\Omega) = [M_{CEST}(-\Omega) - M_{CEST}(\Omega)]/M_{CEST}(-\Omega)$$

7. **CEST MRI** experiments were performed on a Bruker 7 T Biospec scanner with 30 cm bore size on implanted xenograph mammary tumors of mice before and following the injection of the glucose analogs 2-DG or FDG. DA3 tumor bearing mice that were allowed to grow for 10–14 days, with an average tumor volume of 5 mm^3 were scanned. The mice were anesthetized using isoflurane (1–2%) or by injection of ketamine-xylazine (191 mg/kg and 4.25 mg/kg, respectively) and scanned with surface coil. Their temperature was monitored and maintained at 37°C. The injection of the contrast medium, 2-DG or FDG (in saline, pH = 7.4) was performed through the tail vein.

The *in vivo* CEST. Images were generated as follows: a series of gradient-echo images were collected from a single 1 mm axial slice of (acquisition matrix 128 × 64, field of view of 40 × 40 mm^2) after 1.2 s presaturation pulse of 2.5 μT (106 Hz) at ±1.2 ppm from the water signal. In the initial experiments the WASSR method[40] (with 0.5 μT pulse amplitude and offset frequencies within ±0.05 ppm steps) was used in order to correct for possible B_0 shifts. The script for the WASSR in MATLAB was obtained from the F.M. Kirby Research Center. However since the results with and without the WASSR correction were identical the correction was not used in further experiments.

For the MTRasym plot we used the mean intensities within the selected region of interest (ROI) within the tumor.

1. Warburg, O. On the origin of cancer cells. *Science* **123**, 309–314 (1956).
2. Kroemer, G. & Pouyssegur, J. Tumor cell metabolism: cancer's Achilles' heel. *Cancer Cell* **13**, 472–482 (2008).
3. Gatenby, R. A. & Gillies, R. J. Why do cancers have high aerobic glycolysis? *Nat Rev Cancer* **4**, 891–899 (2004).
4. Jain, V. K., Kalia, V. K., Sharma, R., Maharajan, V. & Menon, M. Effects of 2-deoxy-D-glucose on glycolysis, proliferation kinetics and radiation response of human cancer cells. *Int J Radiat Oncol Biol Phys* **11**, 943–950 (1985).
5. Pauwels, E. K. *et al.* FDG accumulation and tumor biology. *Nucl Med Biol* **25**, 317–322 (1998).
6. Foehrenbach, H. *et al.* [Positron emission tomography in clinical oncology]. *Presse Med* **32**, 276–283 (2003).
7. Czernin, J. & Phelps, M. E. Positron emission tomography scanning: current and future applications. *Annu Rev Med* **53**, 89–112 (2002).
8. Kubota, K. From tumor biology to clinical Pet: a review of positron emission tomography (PET) in oncology. *Ann Nucl Med* **15**, 471–486 (2001).
9. Gambhir, S. S. Molecular imaging of cancer with positron emission tomography. *Nat Rev Cancer* **2**, 683–693 (2002).
10. Pichler, B. J., Kolb, A., Nagele, T. & Schlemmer, H. P. PET/MRI: paving the way for the next generation of clinical multimodality imaging applications. *J Nucl Med* **51**, 333–336 (2010).
11. Tanimoto, K. *et al.* Role of glucose metabolism and cellularity for tumor malignancy evaluation using FDG-PET/CT and MRI. *Nucl Med Commun* **31**, 604–609 (2010).
12. Nakada, T., Kwee, I. L., Griffey, B. V. & Griffey, R. H. ^{19}F 2-FDG NMR imaging of the brain in rat. *Magnetic Resonance Imaging* **6**, 633–635 (1988).
13. Kanazawa, Y., Umayahara, K., Shimmura, T. & Yamashita, T. ^{19}F NMR of 2-deoxy-2-fluoro-D-glucose for tumor diagnosis in mice. An NDP-bound hexose analog as a new NMR target for imaging. *NMR Biomed* **10**, 35–41 (1997).
14. Guivel-Scharen, V., Sinnwell, T., Wolff, S. D. & Balaban, R. S. Detection of proton chemical exchange between metabolites and water in biological tissues. *J Magn Reson* **133**, 36–45 (1998).
15. Ward, K. M., Aletras, A. H. & Balaban, R. S. A new class of contrast agents for MRI based on proton chemical exchange dependent saturation transfer (CEST). *J Magn Reson* **143**, 79–87 (2000).
16. Zhou, J. & Zijl, P. C. M. v. Chemical exchange saturation transfer imaging and spectroscopy. *Progress in Nuclear Magnetic Resonance Spectroscopy* **48**, 109–136 (2006).
17. Vinogradov, E., Sherry, A. D. & Lenkinski, R. E. CEST: from basic principles to applications, challenges and opportunities. *J Magn Reson* **229**, 155–172 (2013).
18. Liu, G., Song, X., Chan, K. W. & McMahon, M. T. Nuts and bolts of chemical exchange saturation transfer MRI. *NMR Biomed* (2013).
19. Zhou, J. Y., Payen, J. F., Wilson, D. A., Traystman, R. J. & van Zijl, P. C. M. Using the amide proton signals of intracellular proteins and peptides to detect pH effects in MRI. *Nat Med* **9**, 1085–1090 (2003).
20. Zhou, J., Lal, B., Wilson, D. A., Laterra, J. & van Zijl, P. C. Amide proton transfer (APT) contrast for imaging of brain tumors. *Magn Reson Med* **50**, 1120–1126 (2003).
21. van Zijl, P. C., Jones, C. K., Ren, J., Malloy, C. R. & Sherry, A. D. MRI detection of glycogen in vivo by using chemical exchange saturation transfer imaging (glycoCEST). *Proc Natl Acad Sci U S A* **104**, 4359–4364 (2007).
22. Haris, M., Cai, K., Singh, A., Hariharan, H. & Reddy, R. In vivo mapping of brain myo-inositol. *Neuroimage* **54**, 2079–2085 (2011).
23. Gilad, A. A. *et al.* Artificial reporter gene providing MRI contrast based on proton exchange. *Nat Biotechnol* **25**, 217–219 (2007).
24. Ling, W., Regatte, R. R., Navon, G. & Jerschow, A. Assessment of glycosaminoglycan concentration in vivo by chemical exchange-dependent saturation transfer (gagCEST). *Proc Natl Acad Sci U S A* **105**, 2266–2270 (2008).
25. Saar, G. *et al.* Assessment of glycosaminoglycan concentration changes in the intervertebral disc via chemical exchange saturation transfer. *NMR Biomed* **25**, 255–261 (2012).
26. Chan, K. W. *et al.* Natural D-glucose as a biodegradable MRI contrast agent for detecting cancer. *Magn Reson Med* **68**, 1764–1773 (2012).
27. Walker-Samuel, S. *et al.* In vivo imaging of glucose uptake and metabolism in tumors. *Nat Med* **19**, 1067–1072 (2013).
28. Nasrallah, F. A., Pages, G., Kuchel, P. W., Golay, X. & Chuang, K. H. Imaging brain deoxyglucose uptake and metabolism by glucoCEST MRI. *J Cereb Blood Flow Metab* **33**, 1270–1278 (2013).
29. Kanazawa, Y. *et al.* Metabolic pathway of 2-deoxy-2-fluoro-D-glucose studied by F-19 NMR. *Life Sci* **39**, 737–742 (1986).
30. Kojima, M. *et al.* Metabolic pathway of 2-deoxy-2-fluoro-D-glucose and 2-deoxy-2-fluoro-D-mannose in mice bearing sarcoma 180 studied by fluorin-19 nuclear magnetic resonance. *Chem Pharm Bull (Tokyo)* **36**, 1194–1197 (1988).
31. Rigo, P. *et al.* Oncological applications of positron emission tomography with fluorine-18 fluorodeoxyglucose. *Eur J Nucl Med* **23**, 1641–1674 (1996).

32. Carnochan, P. & Brooks, R. Radiolabelled 5′-iodo-2′-deoxyuridine: a promising alternative to [18F]-2-fluoro-2-deoxy-D-glucose for PET studies of early response to anticancer treatment. *Nucl Med Biol* **26**, 667–672 (1999).
33. Navon, G., Lyon, R. C., Kaplan, O. & Cohen, J. S. Monitoring the transport and phosphorylation of 2-deoxy-D-glucose in tumor cells in vivo and in vitro by 13C nuclear magnetic resonance spectroscopy. *FEBS Lett* **247**, 86–90 (1989).
34. Dienel, G. A. & Cruz, N. F. Synthesis of deoxyglucose-1-phosphate, deoxyglucose-1,6-bisphosphate, and other metabolites of 2-deoxy-D-[14C]glucose in rat brain in vivo: influence of time and tissue glucose level. *J Neurochem* **60**, 2217–2231 (1993).
35. Pelicano, H., Martin, D. S., Xu, R. H. & Huang, P. Glycolysis inhibition for anticancer treatment. *Oncogene* **25**, 4633–4646 (2006).
36. Stein, M. *et al.* Targeting tumor metabolism with 2-deoxyglucose in patients with castrate-resistant prostate cancer and advanced malignancies. *Prostate* **70**, 1388–1394 (2010).
37. Raez, L. E. *et al.* A phase I dose-escalation trial of 2-deoxy-D-glucose alone or combined with docetaxel in patients with advanced solid tumors. *Cancer Chemother Pharmacol* **71**, 523–530 (2013).
38. Dwarakanath, B. S. *et al.* Clinical studies for improving radiotherapy with 2-deoxy-D-glucose: present status and future prospects. *J Cancer Res Ther* **5 Suppl 1**, S21–26 (2009).
39. Fu, Y. X., Watson, G., Jimenez, J. J., Wang, Y. & Lopez, D. M. Expansion of immunoregulatory macrophages by granulocyte-macrophage colony-stimulating factor derived from a murine mammary tumor. *Cancer Res* **50**, 227–234 (1990).
40. Kim, M., Gillen, J., Landman, B. A., Zhou, J. & van Zijl, P. C. Water saturation shift referencing (WASSR) for chemical exchange saturation transfer (CEST) experiments. *Magn Reson Med* **61**, 1441–1450 (2009).

Acknowledgements

We wish to thank Ms. Lital Avraham for her expert help in handling the animals during the MRI experiments and to Dr. Galia Tsarfaty for helpful discussions. We thank the Strauss Center for computational neuroimaging, the Sackler institute for biophysics and the Israel science foundation for the purchase of the MRI system. This work was supported by research grants from the Breast Cancer Research Foundation and the United States-Israel Binational Science Foundation.

Author contributions

M.R. performed all the NMR and the MRI experiments and participated in writing of the manuscript. J.H. was responsible for animal handling and the implantation of the tumor cells. I.T. supervised the biological part of the work and assisted in the design of the experiments. G.N. has conceived the idea of the work, designed the experiments and participated in writing the manuscript.

Additional information

Competing financial interests: The authors declare no competing financial interests.

How to cite this article: Rivlin, M., Horev, J., Tsarfaty, I. & Navon, G. Molecular imaging of tumors and metastases using chemical exchange saturation transfer (CEST) MRI. *Sci. Rep.* **3**, 3045; DOI:10.1038/srep03045 (2013).